
**DIFFRACTION AND SCATTERING
OF IONIZING RADIATIONS**

Peculiarities of Section Topograms for the Multiple Diffraction of X Rays

V. G. Kohn^a and I. A. Smirnova^b

^a National Research Centre “Kurchatov Institute”, pl. Akademika Kurchatova 1, Moscow, 123182 Russia

^b Institute of Solid State Physics, Russian Academy of Sciences, Chernogolovka, Moscow oblast, 142432 Russia

e-mail: kohnvict@yandex.ru

Received October 5, 2015

Abstract—The distortion of interference fringes on the section topograms of single crystal due to the multiple diffraction of X rays has been investigated. The cases of the 220 and 400 reflections in a silicon crystal in the form of a plate with a surface oriented normally to the [001] direction are considered both theoretically and experimentally. The same section topogram exhibits five cases of multiple diffraction at small azimuthal angles for the 400 reflection and MoK α radiation, while the topogram for the 220 reflection demonstrates two cases of multiple diffraction. All these cases correspond to different combinations of reciprocal lattice vectors. Exact theoretical calculations of section topograms for the aforementioned cases of multiple diffraction have been performed for the first time. The section topograms exhibit two different distortion regions. The distortions in the central region of the structure are fairly complex and depend strongly on the azimuthal angle. In the tails of the multiple diffraction region, there is a shift of two-beam interference fringes, which can be observed even with a laboratory X-ray source.

DOI: 10.1134/S1063774516040118

INTRODUCTION

The section topography of silicon single crystals of high structural quality makes it possible to detect and successfully identify individual structural defects (e.g., dislocations and stacking faults) by analyzing their influence on the interference pattern of a perfect crystal via far strain fields. The corresponding method was proposed by Kato and Lang [1]. Its essence is as follows. A narrow slit of width d is installed before a crystal to limit the incident X-ray beam in one direction. The beam expands due to the dynamic diffraction in the crystal. This expansion leads to the illumination of the so-called Borrmann fan, formed by the vectors of the incident (\mathbf{s}_0) and reflected (\mathbf{s}_h) waves. If crystal thickness t is sufficiently large, the width of the reflected beam in the perpendicular direction becomes equal to $D = d + 2t \sin \theta_B \gg d$.

The interference of the incident and reflected waves leads to the occurrence of bright- and dark-contrast fringes; note that the distance between the fringes in the central part of the pattern exceeds the slit size, which is why the slit does not deteriorate the central interference fringes even in for X-ray beams with low spatial coherence. The crystal structure defects may distort fringes because of the lattice strain. However, there is another source of fringe distortion even in the absence of defects. If the source angular size is small along a fringe, different parts of the topogram in this

direction correspond to different azimuthal angles. Some angles provide conditions for multiple diffraction, due to which other reflected beams arise. Fringe distortion occurs due to the change in the character of interaction between the X-ray beam and crystal.

The multiple diffraction theory was initially developed for a plane incident wave and an infinite crystal plate [2–4]. It studies the angular dependences of the incident beam reflection. The angular dependences for a thick crystal in the Laue (transmission) geometry have a very fine structure, which can be resolved using only precise collimators [5–7]. In a laboratory experiment, section topography makes it possible to investigate multiple diffraction using simple tools; however, in this case, it is necessary to calculate the Fourier transform with respect to the polar angle after calculating the angular dependence.

The specific features of section topograms in the case of multiple diffraction were studied in [8] using synchrotron radiation with a high resolution in the azimuthal angle, however, no exact theoretical calculations were performed. Such a calculation was performed in [9] for three cases of multiple diffraction, revealed for the 400 reflection in a topogram of a silicon crystal with a surface oriented perpendicular to the [001] direction. The calculation results turned out to be in good agreement with the fringe pattern obtained using a laboratory source with a low resolution in the azimuthal angle. This study is a continua-

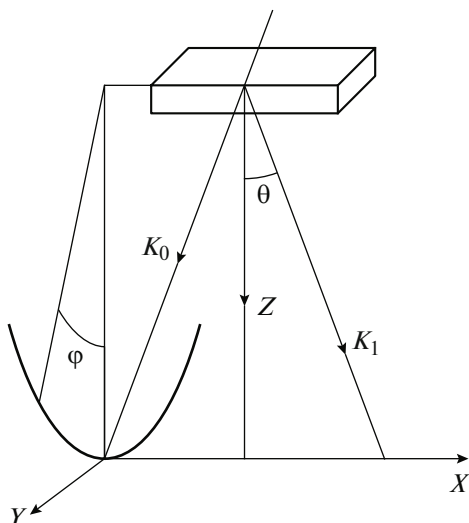


Fig. 1. Geometric scheme of diffraction for section topography, which determines angles θ and φ (\mathbf{k}_0 is the wave vector of incident wave and \mathbf{k}_1 is the wave vector of reflected wave in the two-beam case).

tion of [9]. Here, we report the results of analyzing two more cases of multiple diffraction (revealed in a topogram for the 400 reflection) and two cases for the 220 reflection.

The advantage of the experimental scheme under consideration is that all cases of multiple diffraction are observed on the same topogram without crystal rotation. The problem of determining additional reflections from a known value of azimuthal angle itself is of importance. Below we present the solution to this problem and a method for calculating topograms.

THEORY AND CALCULATION METHOD

When searching for additional reflections on a section topogram at specified polar angle θ and azimuthal angle φ in planes oriented perpendicular and parallel to the topogram plane, it is convenient to use the crystal coordinate system. In this case, normal \mathbf{n}_0 to the crystal surface is directed along the [001] axis, which is assumed to be Z axis. Correspondingly, the X and Y axes are directed along the [100] and [010] axes of cubic crystal. Angles θ and φ determine the incident beam direction (specifically, the coordinates of variable wave vector \mathbf{k}_0 of incident plane wave (Fig. 1). In this case, one uses other X and Y axes directed parallel and perpendicular to the reciprocal lattice vector.

Both coordinate systems coincide on the section topogram for the 400 reflection, and vector $\mathbf{k}_0 = K\mathbf{s}_0$, $\mathbf{s}_0 = (-\sin \theta, \cos \theta \sin \varphi, \cos \theta \cos \varphi)$, where $K = 2\pi/\lambda$ is the wave number and λ is the X-ray wavelength. Obviously, angle θ is the Bragg angle for the 400 reflection ($\sin \theta = 2\lambda/a$, where a is the lattice constant). The

problem to solve is as follows: with the values of angles θ and φ specified, one must test all reciprocal lattice vectors with Miller indices (n_1, n_2, n_3) and find those satisfying the Bragg conditions in the best way. These conditions can be written as

$$\alpha = (S_x^2 + S_y^2 + S_z^2 - 1) < 10^{-5},$$

$$S_x = -\sin \theta + An_1, \quad S_y = \cos \theta \sin \varphi + An_2, \quad (1)$$

$$S_z = \cos \theta \cos \varphi + An_3$$

where $A = \lambda/a = \sin \theta/2$ and n_1, n_2 , and n_3 are integers. Only even–even or odd–odd combinations can be chosen for a silicon crystal.

It was shown in [9] that a four-wave case (220; 400; $\bar{2}\bar{2}0$) is implemented at $\varphi = 0$, another four-wave case (400; $\bar{5}\bar{3}\bar{1}$; $\bar{1}\bar{3}\bar{1}$) occurs at $\varphi = 4.938$ mrad, and a symmetric case (400; $\bar{5}\bar{3}\bar{1}$; $\bar{1}\bar{3}\bar{1}$) corresponds to $\varphi = -4.938$ mrad. In this paper we additionally present a fragment of experimental topogram and the results of a theoretical calculation for a four-wave case (400; $\bar{6}\bar{4}\bar{2}$; $\bar{2}\bar{4}\bar{2}$), which is implemented at $\varphi = 41.674$ mrad. Correspondingly, there is a symmetric case for the negative value of φ and the vectors with the opposite sign of y component.

Note that a calculation from formulas (1) for each azimuthal angle takes much time. However, the calculation time can be reduced. To this end, it is sufficient to indicate the reciprocal lattice vectors yielding the minimum value of parameter α . Then, using two reciprocal lattice vectors and the specified value of angle θ (i.e., specified radiation wavelength), one can determine the coordinates of vector \mathbf{s}_0 , as was described in [4] and then find (based on these coordinates) the exact value of angle φ , using again formulas (1).

On the section topogram for the 220 reflection, the X axis in the topogram coordinate system (Fig. 1) is parallel to the $c[110]$ axis, and the Y axis is parallel to $c[\bar{1}\bar{1}0]$, where $c = 2^{-1/2} = 0.7071$. The coordinates of vector \mathbf{s}_0 in the crystal coordinate system are $\mathbf{s}_0 = (-c[\sin \theta + \cos \theta \sin \varphi], -c[\sin \theta - \cos \theta \sin \varphi], \cos \theta \cos \varphi)$, and $\sin \theta = \lambda/(ca)$. Correspondingly, parameters S_x and S_y in formula (1) should be replaced with

$$S_x = -c[\sin \theta + \cos \theta \sin \varphi] + An_1,$$

$$S_y = -c[\sin \theta - \cos \theta \sin \varphi] + An_2. \quad (2)$$

A four-wave case (220; $\bar{1}\bar{5}\bar{1}$; $\bar{3}\bar{1}\bar{1}$) was found to be implemented at azimuthal angle $\varphi = 1.1600$ mrad. At a negative value of this angle, the symmetric four-wave case differs from the aforementioned one by the permutation of Miller indices x and y .

Having determined angles θ and φ , one can calculate coordinate y on an experimental topogram at small azimuthal angles from the formula $y = \varphi L \cos \theta$.

It was assumed in [9] that $\cos \theta \approx 1$; however, in the case of section topograms for reflections with large Miller indices (e.g., the 800 reflection) or at larger radiation wavelengths, the factor $\cos \theta$ must be taken into account.

The theoretical calculation of section topograms with allowance for multiple diffraction was performed in two stages. First, we calculated a two-dimensional map of the angular dependence of four diffracted-wave amplitudes for different polarizations of both incident and reflected waves. Then a Fourier transform with respect to the polar angle was carried out and squares of amplitude moduli were summed.

The angular dependence was calculated according to the scheme that was described for the first time in [10] and used in [9]. When an incident plane wave with a wave vector \mathbf{k}_0 enters a crystal, it undergoes refraction, and the wave vector becomes equal to $\mathbf{k}_0 + \varepsilon \mathbf{n}_0/2$. Correspondingly, the diffracted waves have wave vectors $\mathbf{k}_m + \varepsilon \mathbf{n}_0/2$, where $\mathbf{k}_m = \mathbf{k}_0 + \mathbf{h}_m$; \mathbf{h}_m is the m th reciprocal lattice vector for multiple configuration under consideration, which satisfies the Bragg conditions $k_m^2 = k_0^2$.

It is convenient to write the scalar wave amplitudes in the form $\gamma_m E_{ms}$, where $\gamma_m = (\mathbf{k}_m \mathbf{n}_0)$ and the polarization index s takes two values, corresponding to the components of vector \mathbf{E}_m oriented perpendicular to the \mathbf{k}_m direction. In this case, the problem of determining the amplitudes E_{ms} and parameter ε is reduced to the problem on eigenvalues of complex scattering matrix, specifically,

$$\sum_{ns'} G_{mn}^{ss'} E_{ns'} = \varepsilon E_{ms}. \quad (3)$$

The explicit form of the matrix was reported in [9, 10]. In the cases under consideration, all reflected plane waves emerge from the crystal through the same surface as the incident wave; i.e., all parameters $\gamma_m > 0$.

In this case, the elements of the imaginary part of absorption matrix G are much smaller than the elements of its real part. This circumstance makes it possible to solve problem (3) for only the real part and take into account the imaginary part in terms of perturbation theory. Specifically the diagonal elements of the real part of matrix G depend on angles θ and φ . Problem (3) has $2N$ solutions, where N is the number of multiple-diffraction waves. We denote these solutions by index j . According to the perturbation theory, it is sufficient to find only the imaginary part of eigenvalues, which determines absorption coefficients μ_j .

The total electric field induced in the crystal is a superposition of all eigensolutions entering the sum with different weights. These weights are determined from the boundary conditions. In the case under consideration ($\gamma_m > 0$) they can be found analytically. If the incident wave has a polarization p , the amplitude

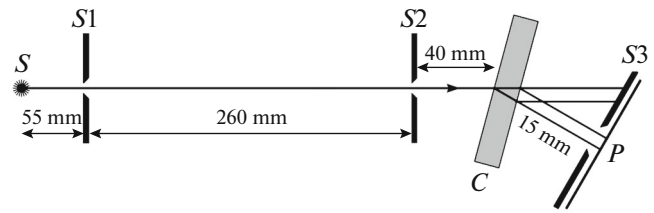


Fig. 2. Schematic of the experiment: (S) X-ray source; (S1–S3) first, second, and third slits; (C) crystal; and (P) photographic plate.

of the reflected wave with polarization s , denoted by subscript m , is

$$R_m^{(p,s)}(\theta, \varphi) = \sum_j E_{0p}^j E_{ms}^j \exp(i\varepsilon t/2), \quad (4)$$

where t is the crystal thickness.

A calculation for this reflection yields four functions, each of which depends on angles θ and φ . As was shown in [9], under laboratory conditions, the slit can be considered an incoherent source, each point of which emits independently. In this case, one must calculate the Fourier transform with respect to variable $q = K\theta$, i.e., pass to the functions

$$U_m^{(p,s)}(x, \varphi) = \int \frac{dq}{2\pi} R_m^{(p,s)}(q, \varphi) \exp(iqx) \quad (5)$$

and then calculate half the sum of the squares of moduli of all four functions.

Transform (5) corresponds to Kato's spherical wave theory [11]], which is valid if distance L_s between the slit and crystal is smaller than $0.1L_f$, where L_f is the diffraction focal length [12]. If this condition is not satisfied, it is necessary to use the more general theory, which was developed in [13, 14]. The pattern obtained from formula (5) corresponds to the ideal experimental conditions: infinitely narrow slit and infinitely small source size in angle φ . To perform a comparison with the results of real experiment, one must average the pattern over the slit width and angular source size.

EXPERIMENTAL

A schematic of the experiment is shown in Fig. 2. We used a laboratory source ($28 \times 30 \mu\text{m}$ in size) of unpolarized MoK_α radiation. Topograms were recorded with a Lang camera (A-3 model). The distances are indicated in the figure. The widths of the first, second, and third slits are, respectively, $400 \mu\text{m}$, $10\text{--}15 \mu\text{m}$, and about 1 mm ; however, the topogram sizes are smaller than 1 mm and depend on the crystal thickness.

Figure 3 shows a fragment of section topogram for the 220 reflection, the central part of which (in the vertical direction) corresponds to the azimuthal angle $\varphi = 1.1600 \text{ mrad}$. Using the above-described method,

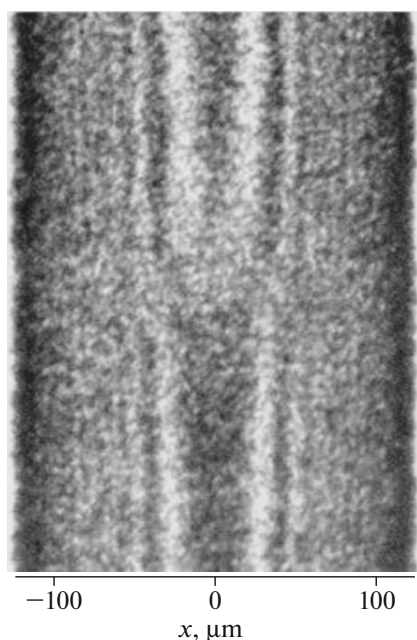


Fig. 3. Fragment of experimental section topogram for the 220 reflection (670- μm -thick crystal, MoK_α radiation) corresponding to multiple diffraction at an azimuthal angle of 1.16 mrad.

we found that this angle corresponds to the four-wave case (220; $\bar{151}$; $\bar{311}$). In this experiment, the crystal thickness is $t = 670 \mu\text{m}$ and the Bragg angle is $\theta = 10.644^\circ$. Correspondingly, the topogram width (Borrmann fan base) is 248 μm .

Although the experimental scheme has a relatively low resolution, one can clearly see the central bright fringes are narrower in the top part of the pattern and wider in the bottom part. This behavior is a consequence of multiple diffraction.

The fragment of the section topogram for the 400 reflection, corresponding to the azimuthal angle $\varphi = 41.674 \text{ mrad}$, is shown in Fig. 4. It corresponds to the four-wave case (400; $\bar{642}$; $\bar{242}$). In this experiment, crystal thickness $t = 1006 \mu\text{m}$, Bragg angle $\theta = 15.142^\circ$, and topogram width is 526 μm . Since the Bragg angle and crystal thickness are larger by a factor of 1.5 in this case than in the previous situation, it is no wonder that the topogram contains a larger number of bright fringes. Despite the grain structure of the image recorded on a photographic plate, one can see many fringes with a small period.

It is of interest that in this case the contrast in the multiple diffraction region has an opposite structure than Fig. 3. Specifically, when approaching this region, the spacing between the fringes increases in the top part and decreases in the bottom part. In [9] we reported the result for the same reflection but smaller azimuthal angle: $\varphi = 4.938 \text{ mrad}$, which corresponds to another system of reciprocal lattice vectors (400;

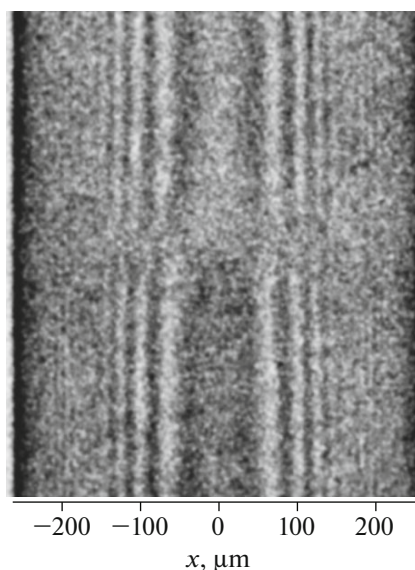


Fig. 4. Fragment of experimental section topogram for the 400 reflection (1006- μm -thick crystal, MoK_α radiation) corresponding to multiple diffraction at an azimuthal angle of 41.76 mrad.

531; $\bar{131}$). The asymmetry is the same as in Fig. 4. Note that the situation presented in Fig. 4 differs from that considered in [9] by the increase in all Miller indices of additional vectors by unity, with the sign preserved.

CALCULATION RESULTS

The angular dependences of functions $R_1^{(ps)}(\theta, \varphi)$ were calculated on a grid containing 2048×161 points. Here, subscript 1 corresponds to the 220 and 400 reflections of the section topograms under consideration. Angle θ is changed inside the intervals 152 and 90 μrad for the 220 and 400 reflections, respectively. The Fourier transform with respect to angle θ was performed using the standard fast Fourier transform (FFT) procedure. The figures show a quarter of the calculation domain.

Figure 5a shows a calculated section topogram for the 220 reflection computed by the above-described method. This topogram corresponds to a slit of infinitely small size and a source with infinitely small angular size. One can see that the size of the multiple region on the azimuthal angle axis does not exceed 60 μrad . The intensity distribution in this region is very complex; its experimental analysis calls for a very high resolution in azimuthal angle.

The two-beam diffraction fringes exhibit bending in the region about 200 μrad in size (with the central part excluded). The Bragg conditions for additional reflections are poorly satisfied in this region; their role is reduced to simple renormalization of scattering parameters. An effect of this type was discussed for the

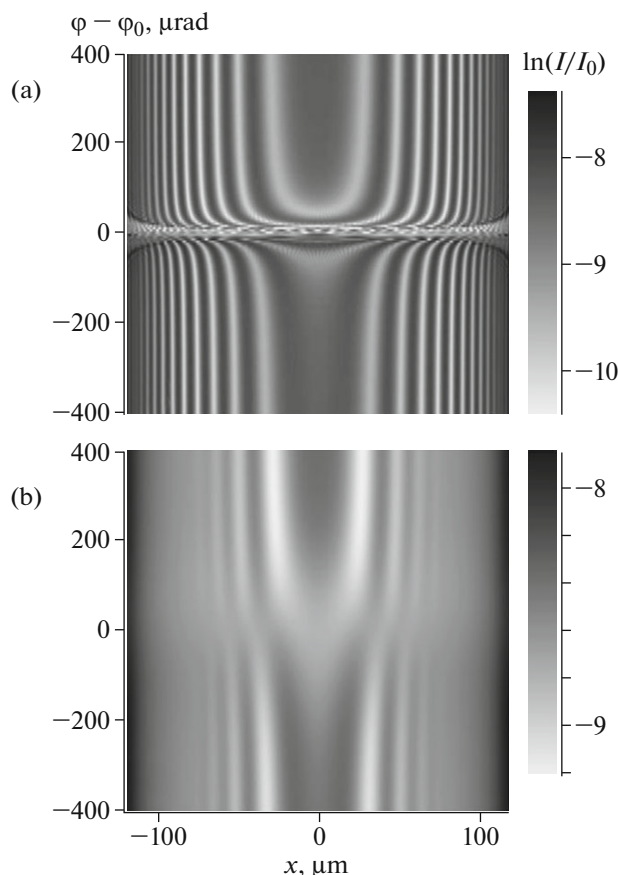


Fig. 5. Theoretical section topogram for the 220 reflection in the multiple diffraction region: (a) a fragment corresponding to infinitely narrow slit and infinitely small angular source width and (b) a fragment obtained with allowance for the finite slit width ($10\ \mu\text{m}$) and angular source size ($40\ \mu\text{rad}$).

first time in [15]. Although strong renormalization is implemented in a wider range of azimuthal angles, it is nevertheless finite. A very weak renormalization is observed in a wider angular range. A multiple diffraction region with a smaller step was presented in [9].

In this paper we present a section topogram (Fig. 5b) obtained from Fig. 5a after calculating the convolution with Gaussian functions with half-widths w_x and w_a over the x and φ axes, respectively. We used the following values: $w_x = 10\ \mu\text{m}$ and $w_a = 40\ \mu\text{rad}$. The w_x value is equal to the width slit. However, with a source size of $30\ \mu\text{m}$ and a total distance of $370\ \text{mm}$, the angular source size is $81\ \mu\text{rad}$. The calculation with this size yields a more diffuse pattern than that shown in Fig. 3.

Thus, a comparison of the calculated and experimental topograms on the multiple diffraction region makes it possible to estimate the effective source size along the topogram. In this case, it turned out to be smaller than expected by a factor of 2. This method makes it possible to estimate the effective sizes of not

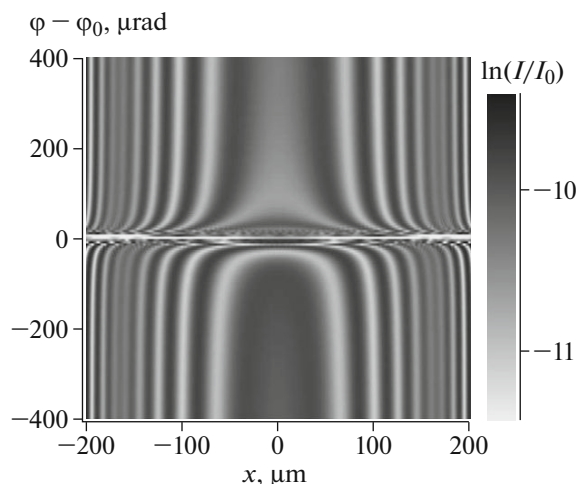


Fig. 6. Theoretical section topogram for the 400 reflection in the multiple diffraction region, centered at an azimuthal angle of $41.674\ \text{mrad}$ ($1006\text{-}\mu\text{m}$ -thick Si crystal, $\text{MoK}\alpha$ radiation, infinitely narrow slit, and infinitely small angular source width).

only laboratory sources, but also synchrotron radiation sources and X-ray free-electron lasers.

It is noteworthy that the multiple diffraction region on the topogram is more sensitive to the crystal thickness than the two-beam region. Therefore, comparing the calculation results and experimental data, one can determine more exactly the local crystal thickness. In particular, it was found that a thickness value of $670\ \mu\text{m}$ is in better correspondence with the experimental data than a value of $680\ \mu\text{m}$, which was expected initially.

Figure 6 shows a theoretical section topogram for the 400 reflection. The calculation was performed for the same parameters as in Fig. 4 but in the ideal case of infinitely narrow slit and infinitely small angular source width. In the tails of the multiple diffraction region, this topogram is the same as in Fig. 2 in [9], although there are differences in the multiple diffraction region. This result is quite expected, because the indices of the additional reciprocal lattice vectors in both cases differ only slightly. The renormalization of two-wave-diffraction parameters is the same, whereas the multiple diffraction region is more sensitive to the indices of additional reflections.

REFERENCES

1. N. Kato and A. R. Lang, *Acta Crystallogr. A* **12**, 178 (1959).
2. A. Authier, *Dynamical Theory of X-ray Diffraction* (Oxford Univ. Press, 2001).
3. S.-L. Chang, *X-Ray Multiple-Wave Diffraction: Theory and Applications*. Springer Series in Solid State Sciences (Springer, Berlin, 2004).

4. Z. G. Pinsker, *X-ray Crystal Optics* (Nauka, Moscow, 1982) [in Russian].
5. A. Kazimirov and V. G. Kohn, *Acta Crystallogr. A* **66**, 451 (2010).
6. A. Kazimirov and V. G. Kohn, *Acta Crystallogr. A* **67**, 409 (2011).
7. V. G. Kohn and A. Kazimirov, *Acta Crystallogr. A* **68**, 331 (2012).
8. F. Heyroth, H.-R. Hoche, and C. Eisenschmidt, *J. Appl. Crystallogr.* **32**, 489 (1999).
9. V. G. Kohn and I. A. Smirnova, *Acta Crystallogr. A* **71**, 519 (2015).
10. V. G. Kohn, *Fiz. Tverd. Tela* **18**, 2538 (1976) [*Sov. Phys. Solid State*, **18**, 1482 (1976)].
11. N. Kato, *Acta Crystallogr.* **14**, 526 (1961).
12. A. M. Afanas'ev and V. G. Kohn, *Fiz. Tverd. Tela* **19**, 1775 (1977).
13. V. G. Kohn, *Fiz. Tverd. Tela* **19**, 3567 (1977). [*Sov. Phys. Solid State*, **19**, 2085 (1977)].
14. V. G. Kohn and A. H. Toneyan, *Acta Crystallogr. A* **42**, 441 (1986).
15. R. Hoier and K. Martinsen, *Acta Crystallogr. A* **39**, 854 (1983).

Translated by Yu. Sin'kov